10^{th} International Conference on Fracture Mechanics of Concrete and Concrete Structures
FraMCoS-X
G. Pijaudier-Cabot, P. Grassl and C. La Borderie (Eds)
https://doi.org/10.21012/FC10.235461

DOUBLE CANTILEVER INDIRECT TENSION FRACTURE TESTING OF CONCRETE

FERHUN C. CANER[*], A. ABDULLAH DÖNMEZ[†], SIDDIK ŞENER[‡] AND VAROL KOÇ[§]

[*]Universitat Politècnica de Catalunya (UPC)
Barcelona, Spain
e-mail: ferhun.caner@upc.edu

[†]İstanbul Technical Üniversitesi (ITÜ)
İstanbul, Turkey
e-mail: donmezab@itu.edu.tr

[‡]İstanbul Bilgi Üniversitesi
İstanbul, Turkey
e-mail: siddik.sener@bilgi.edu.tr

[§]Ondokuz Mayıs Üniversitesi
Samsun, Turkey
e-mail: kvarol@omu.edu.tr

Key words: Double cantilever test, Mode I fracture, Microplane model M7, Size effect

Abstract. The Double Cantilever Beam (DCB) Mode I fracture testing has been widely used in fracture testing of especially fiber reinforced polymer composites and adhesive joints. Application of classical DCB testing to plain concrete or unreinforced ceramic specimens is not straightforward and cannot be carried out in direct separation mode as applied in such composite materials. Instead, in this study an indirect tension approach is proposed for testing concrete in Mode I fracture. Tests of notched geometrically similar DCB specimens made of normal and high strength concretes loaded eccentrically at the cantilever beam-column ends in compression have been carried out. The peak loads from these tests and their classical type II size effect analyses results are reported. The Microplane Model M7 is used to predict and verify the test results. To this end, the model is first calibrated independently of size effect test data using only the uniaxial compression tests. Next, the model M7 is used to predict the peak loads of tested specimens. Furthermore, to determine the errors involved in the size effect fracture parameters, the peak loads of virtual geometrically similar DCB specimens of appropriately chosen sizes were determined using the calibrated model. The same size effect analyses are performed on the predicted peak loads including those from the virtual specimens and the errors in the fracture parameters obtained from the classical size effect analyses of the peak loads obtained from the tests are determined.

1 INTRODUCTION

Double cantilever tension testing has long been a well known method of Mode I fracture testing. It has been applied extensively to polymer composites and adhesive joints and to metals and wood as well. An early application is the DCB tests of Heady [1] in which the critical stress intensity factor for slow crack growth due to corrosion is measured in high strength steels. The analyses of Kanninen [2, 3] are the some of the earliest studies that could match the experimental results only for initial crack extensions. In later studies, higher order plate theories with transverse shear deformation [4] and Timoshenko beam supported on an elastic foundation were used [5–11]. The calculation of energy release rate in the DCB specimens made of fiber reinforced polymer composites loaded in direct Mode I fracture has also been widely studied [12–15]. Finite element analyses of the DCB direct Mode I fracture tests in which sophisticated constitutive models for fiber reinforced polymer composites are employed have been performed as well [16–19]. The DCB direct Mode I fracture tests were also applied to engineering materials such as wood [20] and bovine bone tissue [21], as well as debonding of adhesively bonded joints that produced a large literature (see e.g. [22]).

In all these studies the DCB loading has been a direct separation of the cantilever beams at the free ends to produce Mode I fracture, as given in the standards ASTM D5528-13 [23], ISO 15024 [24] and JIS K7086 [25]. However, this conventional DCB loading configuration would result in two fundamental problems in the case of concrete: (1) Distributed cracking along the cantilever arms that dissipate spurious energy becomes inevitable due to bending moment and shear, (2) the shear stresses acting in the fracture process zone cause the crack to curve resulting in mixed mode fracture instead of pure Mode I fracture.

In this study, size effect tests conducted using a nonconventional loading configuration and fracturing analyses of DCB specimens made of plain normal and high strength concretes loaded to produce Mode I fracture, first presented in [26], are analyzed. In these tests, DCB specimens are supported eccentrically at the cantilever ends and loaded in compression that cause bending moments in the DCB cantilever beam-columns as well as compressive stresses parallel to the initial notch. As opposed to classical separation type loading configuration, the lack of shear in the cantilever arms allow the crack to grow in a straight line and the spurious energy dissipation due to distributed cracking along these arms is prevented. In addition, the test results are analyzed using the Type II Size Effect Law and the errors in the size effect parameters have been determined using the latest version of the Microplane models for concrete called the Microplane model M7.

2 NOVEL DCB SIZE EFFECT TESTS AND ANALYSES

In the three test series named series A, B and C, DCB specimens made of normal and high strength concretes were cast. In each series, three different sizes for the specimens were considered and three specimens were cast for each size. Thus, each series contained nine specimens; since all three series were produced using normal and high strength concrete, in total 54 specimens were cast. The specimens were labelled starting with “P” and “HS” which correspond to plain and high strength DCBs, followed by the series name, i.e. one of the letters A, B and C, and the numbers 1-3, 4-6, 7-9 to identify each of the three specimens. The specimen dimensions were chosen to have 2D geometrical similarity in the ratios 1:2:4. Independently of the size effect tests, the direct tension tensile strengths of the normal strength and high strength concretes are estimated to be $f_t' = 2.40$MPa and $f_t' = 3.20$MPa respectively. The specimen geometries and dimensions are shown in Fig.1. The experimental setup is depicted in Fig. 2a. For more details on the testing program see [26].

In Type II size effect analyses, first the failure loads P_u given in Table 2 of [26] are used to calculate the nominal strengths as $\sigma_{Nu} = P_u/bd$ where b is the width (out of plane dimension) of the specimen and d is the height of the specimen as shown in Fig.2b. For small enough size DCB specimens, the nominal strength must approach a horizontal asymptote (or constant strength) and for large enough size DCB specimens, it must approach the LEFM asymptote with a $-1/2$ slope in the log-log scale. The simplest formula that satisfies both conditions and provides the transition from one extreme to the other may be written as [27]:

$$\sigma_{Nu} = \frac{Bf_t'}{\sqrt{(1 + d/d_0)}} = \frac{\sqrt{E'G_f/g_0'c_f}}{\sqrt{1 + g_0 d/g_0'c_f}} \quad (1)$$

in which Bf_t' = the value of the horizontal asymptote in the small size limit, f_t' = the tensile strength of concrete, G_f = the fracture energy of concrete, $a_{eff} = a_0 + c_f$ = the effective crack length at failure in which a_0 = the notch length and c_f = the half size of the fracture process zone, $g_0 = g(a_0/d)$ = the energy release rate function, $g_0' = g'(a_0/d)$, $E' = E$ = the elastic modulus for plane stress and d_0 = the transitional size between the brittle and strength-limit type behavior for the concrete under consideration.

Eq.1 can be optimally fitted to the test data given in Table 2 of [26] which yields the size effect fracture parameters as given in Table 1. These test data and their optimally fitted size effect curves are plotted in Fig.3. In order to obtain the fracture parameters c_f and G_f, Eqs. 2 and 3 can be obtained starting from Eq.1 as [27]

$$\frac{1}{d_0} = \frac{g_0}{g_0' c_f} \quad (2)$$

$$Bf_t' = \sqrt{\frac{E'G_f}{g_0' c_f}} \quad (3)$$

Furthermore, substituting $c_f = g_0 d_0 / g_0'$ from Eq.2 in Eq.3 one obtains

$$G_f = (Bf_t')^2 \frac{g_0 d_0}{E'} \quad (4)$$

In Fig.2b the nondimensional notch length is given as $\bar{a}_0 = a_0/d = 0.6$, the nondimensional half size of the fracture process zone to be determined from size effect analysis as $\Delta\bar{a} = \Delta a/d$, the nondimensional width of the specimen as $2\bar{c} = 2c/d \approx 0.85$, the nondimensional eccentricity as $\bar{e} = e/d = \bar{c}/5 \approx 0.085$ and the nondimensional notch width as $\bar{\lambda} = \lambda/d$. The nondimensional notch width varied between 0.0167 and 0.0667 because of a constant 5mm notch width employed in all specimens. The nondimensional load is defined as $\bar{P} = P/Ed^2$. In the foregoing equations, E is the Young's modulus and d is the depth of the geometrically similar DCB specimens tested. The nondimensional thicknesses of the specimens $\bar{b} = b/d$ also varied between 0.1 and 0.4 due to different thicknesses of the specimens used in the tests. The effect of such variation in these nondimensional parameters on the results is assumed to be negligible. The energy release rate function value $g_0 = g(0.6)$ and the value of its derivative $g_0' = g'(0.6)$ in the foregoing equations are to be determined for the loading configuration, shape and geometry of the specimens as given above. To this end, the energy release rate is obtained from the complementary strain energy $U^* = P^2C(a)/2$ at constant load:

$$\mathcal{G} = \frac{1}{b}\frac{\mathrm{d}}{\mathrm{d}a}\left[\frac{1}{2}P^2C(a)\right] \quad (5)$$

$$\Rightarrow \mathcal{G} = \frac{1}{2b}\frac{P^2}{d}C'(\bar{a}) \quad (6)$$

where $C(a)$ = the compliance of the structure, i.e. $u = C(a)P$ in which u is the load point displacement and P is the load. The stress intensity factor K_I then is given by

$$K_I = \sigma_N \sqrt{d}\sqrt{g(\bar{a})} = \sqrt{E'\mathcal{G}} \quad (7)$$

where $\sigma_N = P/bd$ is the nominal stress. Substituting $\mathcal{G}$ from Eq.6 into Eq.7 and solving for $g(\bar{a})$ one obtains

$$g(\bar{a}) = \frac{1}{2}E'bC'(\bar{a}) \quad (8)$$

$$\Rightarrow g'(\bar{a}) = \frac{1}{2}E'bC''(\bar{a}) \quad (9)$$

Thus, to determine the value $g_0 = g(\bar{a}_0) = g(0.6)$ one must determine the value $C'(0.6)$ and substitute it in Eq.8. Similarly, to determine the value $g_0' = g'(\bar{a}_0) = g'(0.6)$ one must determine the value $C''(0.6)$ and substitute it in Eq.9. The first and second derivatives of the compliance function can be determined through the finite difference method, which produces highly accurate results [27]. The aforementioned compliances are calculated by linear elastic finite element analyses employing 278400, 272000 and 268800 hexahedral elements of type C3D8R in ABAQUS [28] for all DCB specimens [26].

In Fig.3(a) through (c) the size effect fits for each one of the series PA, PB and PC DCB specimens are given. Similarly, in Figs.3(e) through (g) the size effect fits for each one of the series HSA, HSB and HSC DCB specimens are shown. In Fig.3(d) and Fig.3(h) the size effect fits for all nominal strength data obtained by testing respectively normal strength and high strength DCB specimens are depicted. In Table 1 the size effect fracture parameters obtained through these optimal fits and the foregoing analyses are given.

An important issue is the determination of the errors involved in the experimental results. Typically such a task involves statistical methods applied to error analyses. In this study we attempt to determine the errors in the experimental results by comparing them against realistic numerical analyses results carried out using the microplane model M7. In particular, the errors in the size effect fracture parameters Bf_t', d_0, c_f and G_f, obtained from Type II size effect analyses of the peak loads from the tested specimens are dertermined by comparing them to those obtained from the same analyses applied to the predicted peak loads from the virtual specimens analyzed using the model M7. To improve the numerical predictions of these parameters, a virtual DCB specimen half the size of the smallest tested DCB specimen and a twice as large as the largest tested one are proposed for each test series. The sizes of these virtual specimens are determined based on (1) the computational feasibility of the finite element analyses of the large size virtual specimens, (2) the previous data fitting experience with the Model M7 and (3) the minimum permissible element density in the small size virtual specimens. After calibrating the Model M7 for the two types of concretes employed in the tests using only the elastic moduli and the parameter k_1 of the model M7, the peak loads of all virtual DCB specimens from all series are determined using finite element analyses. As the finite element software, the commercial finite element analysis package ABAQUS version 2016 is employed [28]. The analyses are carried out in the sense of crack band model. The element width is chosen as 2.5mm for both normal and high strength concretes.

The predicted peak loads for the so-called virtual DCB specimens and their optimally fitting size effect curves are shown in Fig.4. For comparison purposes, the experimental peak loads are also shown in the same figure. The optimum values of the size effect fracturing parameters Bf_t', d_0, c_f, G_f and B obtained from the optimal fits of the peak loads from finite element analyses are given in Table 2 for each test series as well as for all normal strength series combined and for all high strength series combined.

Comparing Tables 1 and 2 the errors in the aforementioned parameters may be determined. In particular, the errors in the fracture parameters Bf_t', d_0, c_f, G_f and B obtained using the peak loads from the tests only relative to those obtained using the predicted peak loads from the virtual experiments turn out to be 18.207%, 48.150%, 48.150%, 27.550% and 18.207% for all P-series and 1.664%, 0.344%, 0.344%, 3.000% and 1.664% for all HS-series respectively. Thus, it may be concluded that when the material microstructure is large, the size range that can possibly be tested in the laboratory is likely to be too small compared to the material microstructure size. In such cases the guidance of a well established material model is helpful to obtain reasonable estimates of fracture parameters using the size effect analysis.

In Figs. 5a-e the cracking patterns of the normal strength series C DCB specimens are depicted. The crack propagation is illustrated as the maximum principal logarithmic strain immediately before and immediately after the peak load for each specimen. It is noted that the smallest virtual specimens have the sizes 37.5mm, 50mm and 62.5mm for series A, B and C respectively. Furthermore, the largest virtual specimens have the sizes 600mm, 800mm, 1000mm for series A, B and C respectively. Keeping the element size constant in the sense of crack band model, the normal strength series C DCB specimens depicted in Figs. 5a-e are analyzed using meshes with 1430, 5500, 21000, 84000, and 336000 8-node brick elements of type C3D8R. On the right column in the Fig.5 the half size of the fracture process zone, c_f, is also drawn scaled relative to the size of each DCB specimen to illustrate the equivalent LEFM crack length at peak load. Clearly for the largest virtual DCB specimens, c_f becomes very small.

3 CONCLUSIONS

In this study, test results from a novel DCB indirect Mode I test in which geometrically similar specimens are supported at the cantilever beam-column free ends eccentrically and loaded in compression in the direction of their notches are reported. Employing a sophisticated multiaxial constitutive model for concrete, called the Microplane Model M7 calibrated independently of size effect test data for the normal and high strength concretes employed in the experiments, the experimentally obtained peak loads are predicted. Furthermore, the peak loads of geometrically similar one virtual DCB specimen twice as large as the largest tested DCB specimen and one virtual DCB specimen half the size of the smallest tested DCB specimens in each series are calculated using the finite element analyses with the Model M7. The size effect fracture parameters, namely c_f, G_f, B and d_0 are calculated applying the so-called Bažant's Type II Size Effect Law [29] to peak loads from experiments and also to predicted peak loads from virtual tests. Consequently, we draw the following conclusions:

1. The failure loads obtained from the tests follow the Type II Size Effect Law.

2. The size effect fracture parameters obtained from the failure loads predicted by the Model M7 of geometrically similar virtual DCB specimens are compared to those obtained from the peak loads from the experiments allowing the errors in these experimental results to be estimated.

3. The fracture energy G_f for normal strength concrete turned out to be about 29% higher than that for the high strength concrete when peak loads from experiements only are considered and when peak loads from the virtual specimens are considered, the trend is reversed: G_f for high strength concrete turns out to be higher than that for normal strength concrete by about 11%.

4. In the case of normal strength concrete, the DCB size range tested in the laboratory seems to have remained too small compared to the characteristic size of the material and this leads to errors in excess of 45% in the predicted c_f and over 25% in the predicted G_f; in the case of high strength concrete, these errors respectively are only about 0.34% and about 3%.

5. In contrast to the work of fracture method (in which the full load vs load point displacement diagram must be traced without any snap-back instabilities to yield the two fracture parameters), the proposed DCB indirect Mode I fracture testing method (which involves only the failure loads in compression of geometrically similar DCB specimens to be determined) is vastly simpler because it requieres much less instrumentation.

6. To determine the errors in the size effect fracture parameters, the model M7 must be calibrated independently of the peak loads obtained in the size effect tests using only the free parameters of the model, e.g. using the uniaxial compression tests.

7. In principle instead of the model M7 a cohesive crack can also be introduced in the crack path and the analyses be repeated. However, in this case the calibration of the cohesive law independently of the size effect data will be a defeating problem.

Series	Bf'_t, MPa	d_0, mm	c_f, mm	G_f, N/mm	B
PA	1.466	214.582	25.703	0.052	0.611
PB	1.399	451.081	53.934	0.094	0.583
PC	1.098	723.572	86.836	0.091	0.458
All P's	1.452	255.523	30.608	0.058	0.605
HSA	2.528	90.950	10.894	0.052	0.790
HSB	1.717	228.900	27.369	0.058	0.537
HSC	1.162	878.118	105.384	0.099	0.363
All H's	2.144	114.064	13.663	0.045	0.670

Table 1: The results obtained from fitting $\sigma_{Nu} = Bf'_t/\sqrt{1+d/d_0}$ to the experimental peak loads.

Series	Bf'_t, MPa	d_0, mm	c_f, mm	G_f, N/mm	B
PA	1.807	114.074	13.664	0.042	0.753
PB	1.716	133.192	15.925	0.042	0.715
PC	1.703	127.516	15.303	0.038	0.709
All P's	1.717	132.490	15.870	0.042	0.715
HSA	2.175	119.681	14.336	0.051	0.680
HSB	2.128	120.847	14.449	0.047	0.665
HSC	2.172	103.336	12.401	0.041	0.679
All H's	2.179	113.671	13.616	0.047	0.681

Table 2: The results obtained from fitting $\sigma_{Nu} = Bf'_t/\sqrt{1+d/d_0}$ to the virtual DCB specimen peak loads predicted by the Model M7.

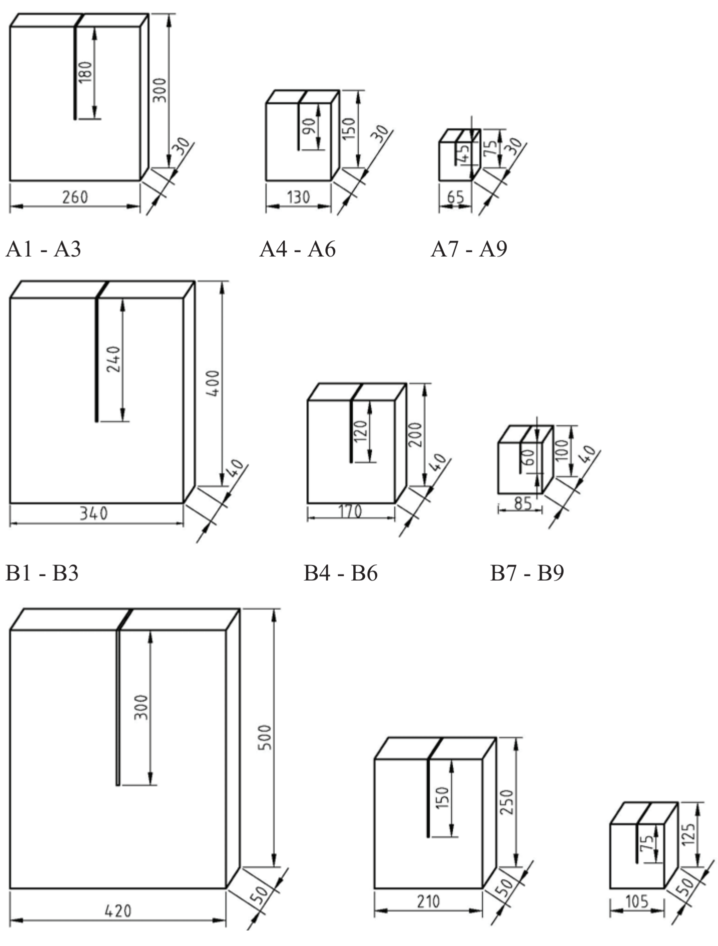

Figure 1: The DCB specimens from the test series A, B and C and their dimensions in mm.

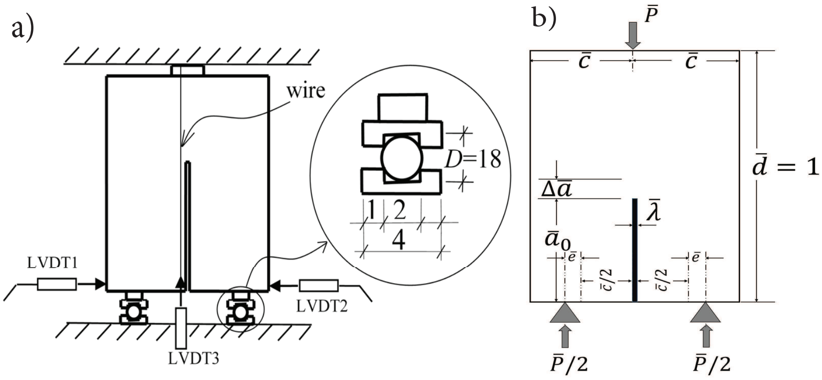

Figure 2: a) The schematic description of the test setup (dimensions in mm), b) the nondimensional dimensions and loading configuration of the indirect tension DCB specimen.

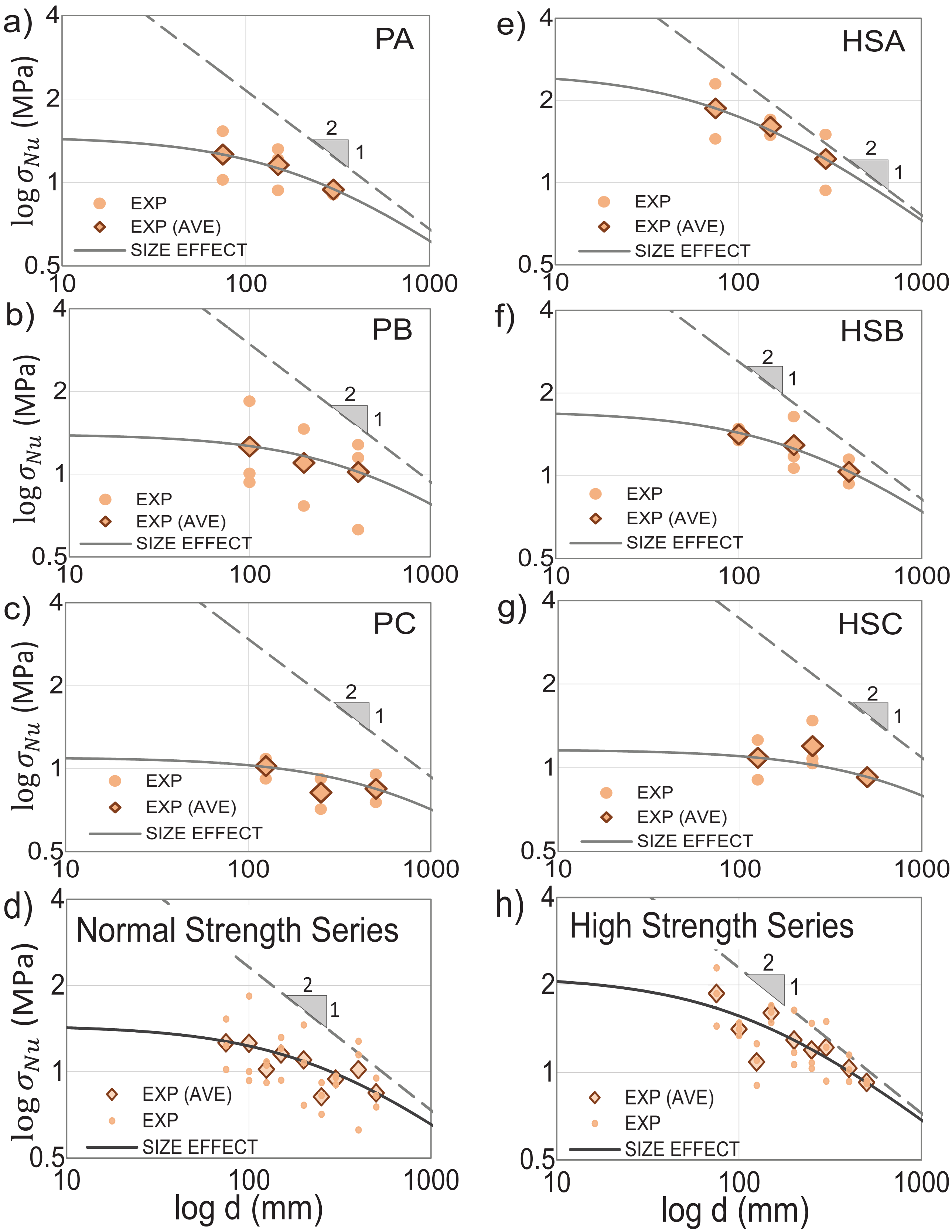

Figure 3: Type II size effect fits to tested DCB specimens for both the normal strength (a-c) and the high strength concretes (e-g) for the series A, B and C; size effect fits to all normal strength DCB specimens combined (d) and to all high strength DCB specimens combined (h).

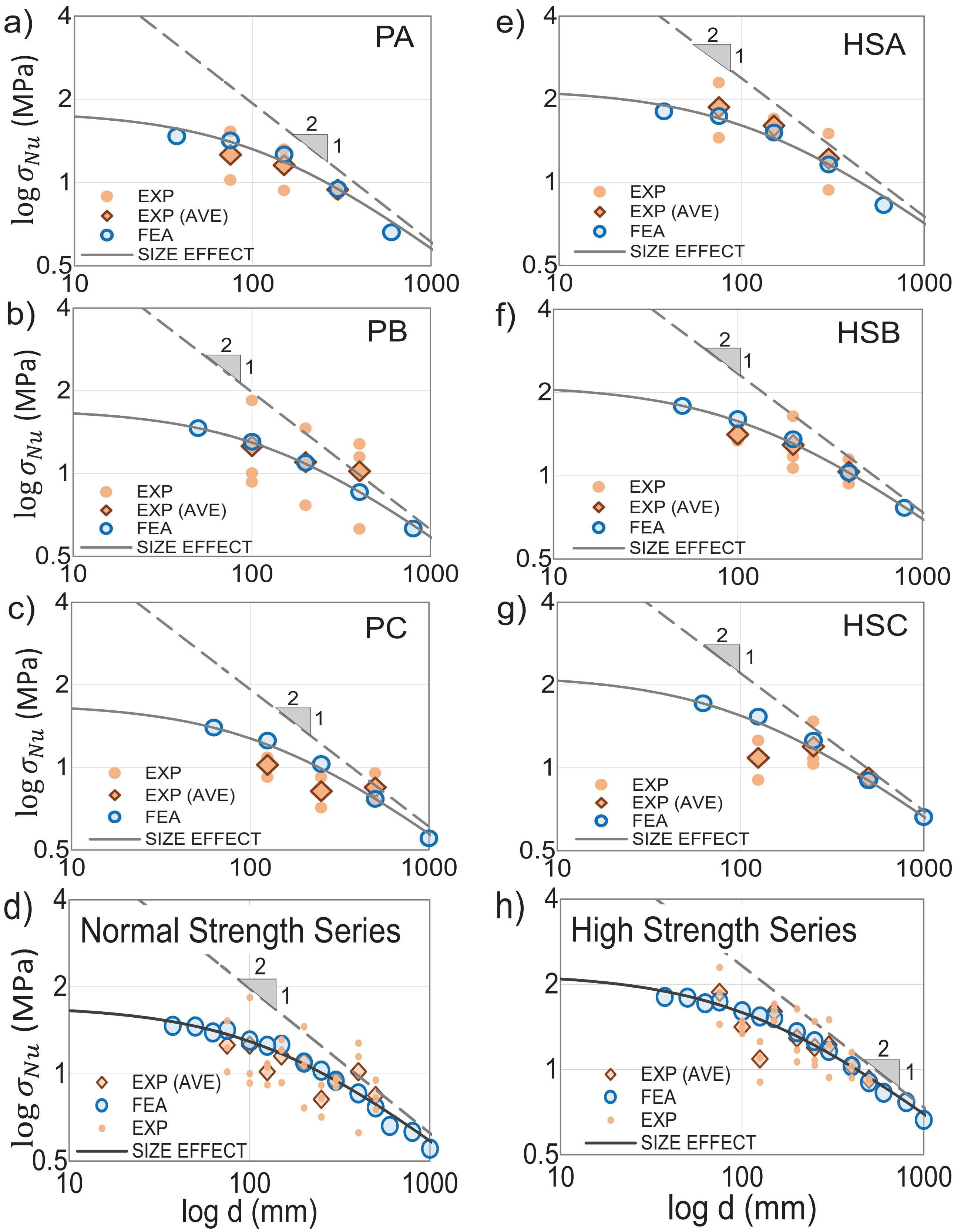

Figure 4: Type II size effect fits to virtual specimen peak loads obtained using the Model M7 for both the normal strength (a-c) and the high strength concretes (e-g) for the series A, B and C; size effect fits to all normal strength virtual DCB specimens (d) and to all high strength virtual DCB specimens (h).

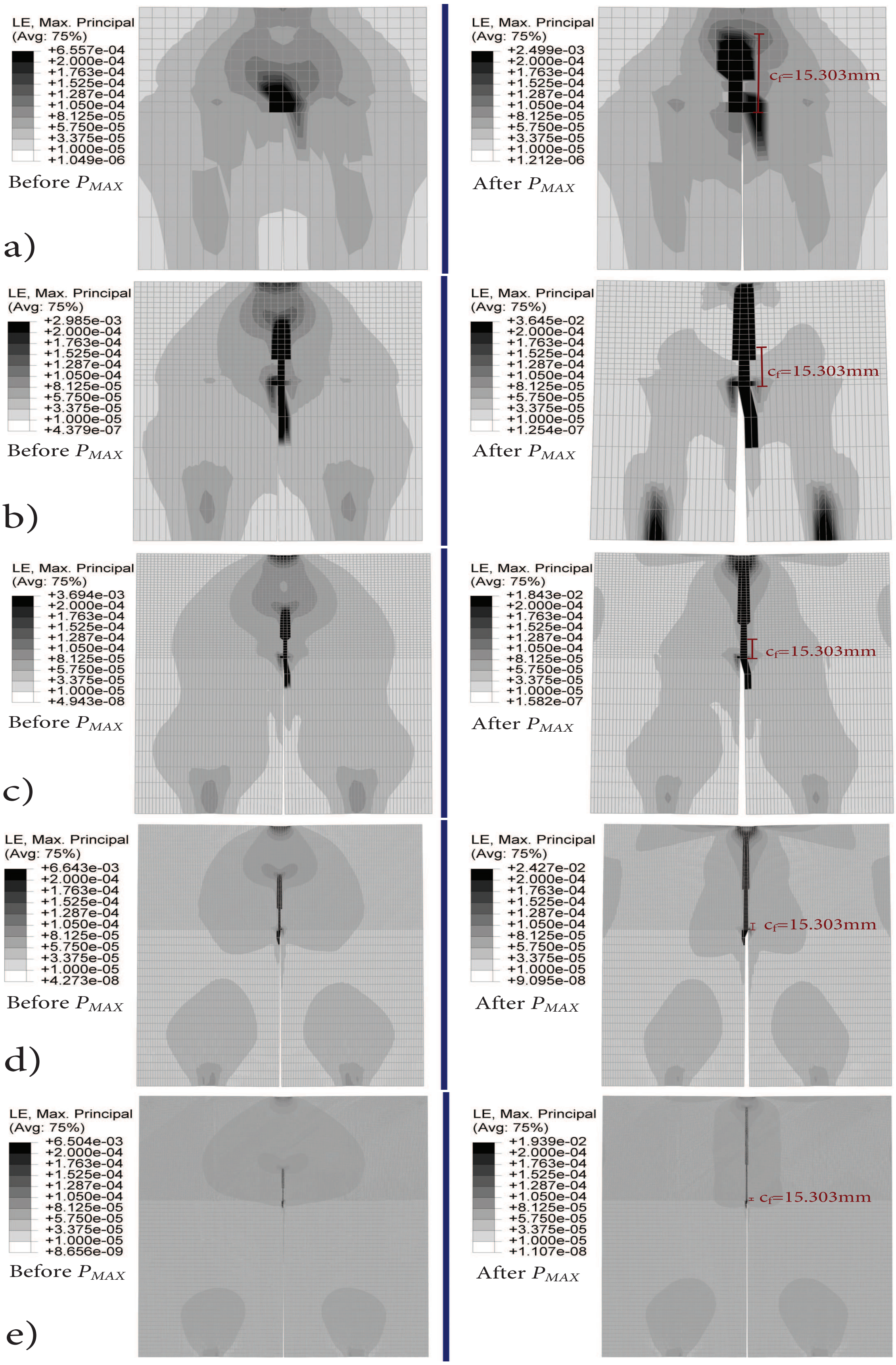

Figure 5: Fracture patterns of DCB specimens for the normal strength concrete specimen sizes of a) $d = 62.5$mm, b) $d = 125$mm, c) $d = 250$mm, d) $d = 500$mm, e) $d = 1000$mm obtained using the Microplane Model M7 with c_f is drawn relative to the specimen size on each specimen on the right.

REFERENCES

[1] R.B. Heady. Evaluation of sulfide corrosion cracking resistance in low alloy steels. *Corrosion*, 33(3):98–107, 1977.

[2] MF Kanninen. An augmented double cantilever beam model for studying crack propagation and arrest. *International Journal of fracture*, 9(1):83–92, 1973.

[3] MF Kanninen. A dynamic analysis of unstable crack propagation and arrest in the dcb test specimen. *International Journal of Fracture*, 10(3):415–430, 1974.

[4] JM Whitney. Stress analysis of the double cantilever beam specimen. *Composites Science and Technology*, 23(3):201–219, 1985.

[5] LB Freund. A simple model of the double cantilever beam crack propagation specimen. *Journal of the Mechanics and Physics of Solids*, 25(1):69–79, 1977.

[6] JG Williams. End corrections for orthotropic dcb specimens. *Composites Science and Technology*, 35(4):367–376, 1989.

[7] S Hashemi, AJ Kinloch, and JG Williams. Corrections needed in double-cantilever beam tests for assessing the interlaminar failure of fibre-composites. *Journal of Materials Science Letters*, 8(2):125–129, 1989.

[8] K. Kondo. Analysis of double cantilever beam specimen. *Advanced Composite Materials*, 4(4):355–366, 1995.

[9] BRK Blackman, H Hadavinia, AJ Kinloch, M Paraschi, and JG Williams. The calculation of adhesive fracture energies in Mode I: revisiting the tapered double cantilever beam (tdcb) test. *Engineering Fracture Mechanics*, 70(2):233–248, 2003.

[10] MM Shokrieh, M Heidari-Rarani, and MR Ayatollahi. Calculation of g_i for a multidirectional composite double cantilever beam on two-parametric elastic foundation. *Aerospace Science and Technology*, 15(7):534–543, 2011.

[11] MM Shokrieh and A Zeinedini. A novel method for calculation of strain energy release rate of asymmetric double cantilever laminated composite beams. *Applied Composite Materials*, 21(3):399–415, 2014.

[12] DJ Nicholls and JP Gallagher. Determination of g_{Ic} in angle ply composites using a cantilever beam test method. *Journal of Reinforced Plastics and Composites*, 2(1):2–17, 1983.

[13] BD Davidson. An analytical investigation of delamination front curvature in double cantilever beam specimens. *Journal of Composite Materials*, 24(11):1124–1137, 1990.

[14] B Nageswara Rao and AR Acharya. Evaluation of fracture energy g_{Ic} using a double cantilever beam fibre composite specimen. *Engineering Fracture Mechanics*, 51(2):317–322, 1995.

[15] Alfredo Balac de Morais. Double cantilever beam testing of multidirectional laminates. *Composites Part A: Applied Science and Manufacturing*, 34(12):1135–1142, 2003.

[16] AB De Morais, MF De Moura, JPM Gonçalves, and PP Camanho. Analysis of crack propagation in double cantilever beam tests of multidirectional laminates. *Mechanics of Materials*, 35(7):641–652, 2003.

[17] TA Sebaey, N Blanco, CS Lopes, and J Costa. Numerical investigation to prevent crack jumping in double cantilever beam tests of multidirectional composite

laminates. *Composites Science and Technology*, 71(13):1587–1592, 2011.

[18] AB De Morais. A new fibre bridging based analysis of the double cantilever beam (dcb) test. *Composites Part A: Applied Science and Manufacturing*, 42(10):1361–1368, 2011.

[19] B Krull, J Patrick, K Hart, S White, and N Sottos. Automatic optical crack tracking for double cantilever beam specimens. *Experimental Techniques*, 40(3):937–945, 2016.

[20] MFSF De Moura, JJL Morais, and N Dourado. A new data reduction scheme for Mode I wood fracture characterization using the double cantilever beam test. *Engineering Fracture Mechanics*, 75(13):3852–3865, 2008.

[21] J.J.L. Morais, M.F.S.F. de Moura, F.A.M. Pereira, J. Xavier, Dourado N., and J.M.T. Dias, M.I.R.and Azevedo. The double cantilever beam test applied to Mode I fracture characterization of cortical bone tissue. *Journal of the Mechanical Behavior of Biomedical Materials*, 3(6):446–453, 2010.

[22] R Dimitri, P Cornetti, V Mantič, and L. de Lorenzis. Mode I debonding of a double cantilever beam: A comparison between cohesive crack modeling and finite fracture mechanics. *Int. J. of Solids and Structures*, 124:57–72, 2017.

[23] ASTM Standard D5528-13. Standard test method for Mode I interlaminar fracture toughness of unidirectional fiber-reinforced polymer matrix composites, 2013.

[24] ISO 15024. Fibre-reinforced plastic composites - determination of Mode I interlaminar fracture toughness, g_{Ic}, for unidirectionally reinforced materials, 2001.

[25] JIS K 7086. Testing methods for interlaminar fracture toughness of carbon fibre reinforced plastics, 1993.

[26] Ferhun C Caner, A Abdullah Dönmez, Sıddık Şener, and Varol Koç. Double cantilever indirect tension testing for fracture of quasibrittle materials. *Int. Journal of Solids and Structures*, 162:76–86, 2019.

[27] Z.P. Bažant and J. Planas. *Fracture and size effect in concrete and other quasibrittle materials*. CRC Press, London, 1997.

[28] Simulia. Abaqus/Explicit version 2016. *Dassault Systèmes*, 2016.

[29] Zdeněk P Bažant. *Scaling of structural strength*. Hermes- Penton Science Ltd., London, 2005.